Evolution of elastic heterogeneity during aging in metallic glasses

Yue Fan,[1,*] Takuya Iwashita,[2] and Takeshi Egami[1,2,3]

[1]*Materials Science and Technology Division, Oak Ridge National Laboratory, Oak Ridge, Tennessee 37831, USA*
[2]*Department of Physics and Astronomy, Joint Institute for Neutron Sciences, University of Tennessee, Knoxville, Tennessee 37996, USA*
[3]*Department of Materials Science and Engineering, University of Tennessee, Knoxville, Tennessee 37996, USA*

The properties of glasses vary widely depending on the way they are prepared, even though their structures appear similar. We show that the local potential energy landscape (PEL) sensitively reflects the stability differences through simulation of local structural excitation in a model metallic glass. It is observed that the spectrum of local structural excitation develops a pseudogap at low energies as the glass becomes more stable. We also demonstrate that the spatial variation of the atomic level shear modulus, rather than the distribution of the magnitude of the single atom shear modulus, is more closely related to the nature of the PEL and the stabilities of glasses. In particular, local aggregation of atoms with low shear modulus greatly contributes to instability of the system.

I. INTRODUCTION

When a liquid is supercooled without crystallization its viscosity increases rapidly in many cases, ending up with a glass. The underlying reason for this increase is the fact that the structure of a liquid varies with temperature. The mechanism of such a rapid increase in viscosity and structural variation are not well understood at the atomistic level in spite of extensive studies [1]. An effective approach to this problem is to consider the potential energy landscape (PEL) of a liquid [2] and its inherent structure obtained by quenching the liquid very rapidly [3]. But whereas the PEL is a powerful concept, it is a highly multidimensional object, and it is not easy to calculate it or even to visualize it. Especially for the glassy state systematic studies on PEL have been made only recently [4–6]. In this paper through simulation on a model metallic glass we show that the distribution of the activation energies for structural excitation in the PEL reflects the difference among the inherent structures more clearly than the structure, for instance expressed by the atomic pair-density function (PDF). On the other hand, the mechanical properties of the amorphous system are known to be related to elastic heterogeneities [7–11]. Nevertheless, no thorough studies have been made on how the nature of the elastic heterogeneity changes for the systems with different stabilities and aging histories. In this paper, by comparing the quantitative differences of the elastic properties at the atomic scale in two systems with different aging histories, we demonstrate the stabilities of metallic glasses are more strongly affected by the manner with which atoms are organized, rather than the single atomic properties. In particular, only the distributions of soft atoms in the lowest 5 percentile soft atoms are significantly related to the dynamics and stabilities of the system.

II. SYSTEMS SETUP AND SIMULATION PROCEDURES

We consider a metallic model system $Zr_{44}Cu_{56}$ containing 2000 atoms, interacting with an embedded-atom method (EAM) potential [12]. The dimensions of the system are 32.43 Å $\times$ 32.43 Å $\times$ 32.43 Å, and periodic boundary conditions are applied to all three directions. We prepared two starting models, systems I and II. System I is the inherent structure of a liquid at 2000 K, which is far above the glass transition temperature ($\sim$700 K). We first equilibrate the system at 2000 K, and then make an instant quench through the steepest descent algorithm. System II represents a relatively more stable glass. The system is first annealed at 1000 K, and then quenched to zero temperature with a cooling rate of 10^{12} K/s. The potential energy of system II is about 0.015 eV per atom ($\sim$0.3%) lower than system I. All the simulations are under fixed volume conditions. To characterize the local structure in these systems we calculated the atomic-level stresses [13] and atomic-level elastic moduli [14] (see Appendix A 1 for details).

To explore the underlying PEL, including the minima and surrounding saddle points, we mainly employ the activation-relaxation technique (ART), which was initially proposed by Barkema *et al.* [15], and further improved by Cances *et al.* [16]. The prepared two systems serve as the initial configurations in ART. In order to study the local excitations of the system, the initial perturbations in ART are introduced to a small group of atoms with local connectivity [17]. Specifically, we select an atom as the central atom, then randomly displace this atom and its first nearest neighbors, defined by the cutoff between the first and second peaks in the PDF. The magnitude of displacement is fixed at 0.5 Å, while the direction is randomly chosen. When the curvature of PEL is found to be less than -0.01 eV/Å [2], the system is relaxed to the saddle point using the Lanczos algorithm [16]. The saddle point convergence criterion is fulfilled when the overall force of the total system is less than 0.05 eV/Å. The corresponding activation energy is thus the difference between the saddle point energy and the initial state energy. For each group of atoms, we employ 10 ART searches with different random perturbation directions. Since there are 2000 such groups in our modeling system, that overall provides 20 000 searches by ART. After removing the failed searches and redundant saddle points, 2200 different activations, on average, are identified for each of the prepared two systems.

*Corresponding author: fany@ornl.gov
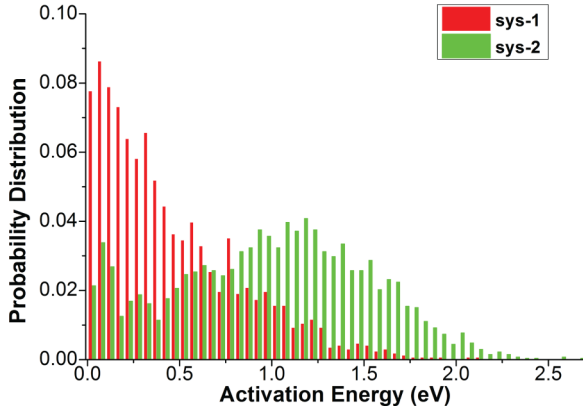
FIG. 1. (Color online) The probability distributions of the activation energies in two systems with different stabilities. Red (dark) bars are the results for system I, the inherent structure of a liquid at 2000 K, while the green (light) bars represent system II, a glass obtained by relatively slow cooling.

III. RESULTS

The histograms of the activation barriers for the two systems are shown in Fig. 1. It can be seen that the two systems have very different distributions of activation barrier height. For system I, i.e., the inherent structure of a liquid at 2000 K, the distribution almost monotonically decreases with energy and

has a large fraction of low-energy activations. For system II, on the other hand, the overall distribution is shifted to higher energy with a peak at 1.2 eV, and the low-energy activations are significantly suppressed. It is worth noting that no external loadings is involved in the present study, and Fig. 1 essentially represents the energy spectra for thermal activations. If large external loading is applied, the behaviors of the system would be determined by the complicated coupling between thermal activation and external loading [18]. Whereas such coupling can be well described in crystalline materials [19–21], it still remains challenging in amorphous systems [18]. The effects of large external loading are beyond the scope of the present study, and hence we focus our discussions below on the thermal activation spectra.

The results in Fig. 1 indicate that the two systems have significantly different stabilities in both aspects of thermodynamics and kinetics [18]. In particular, system I is much less stable than system II because system I has a higher potential energy (thermodynamically unstable) and a larger fraction of low-energy activations (kinetically unstable). This comparison between the two systems is consistent with the previous studies by Rodney *et al.* [4,18,22] albeit in different materials and different dimensions, where they show there is much higher fraction of low-energy activations in an unstable (flowing) system than in a stable system. In the present study, the cooling rate of system II, 10^{12} K/s, is still very high and the system is not yet well relaxed. With lower cooling
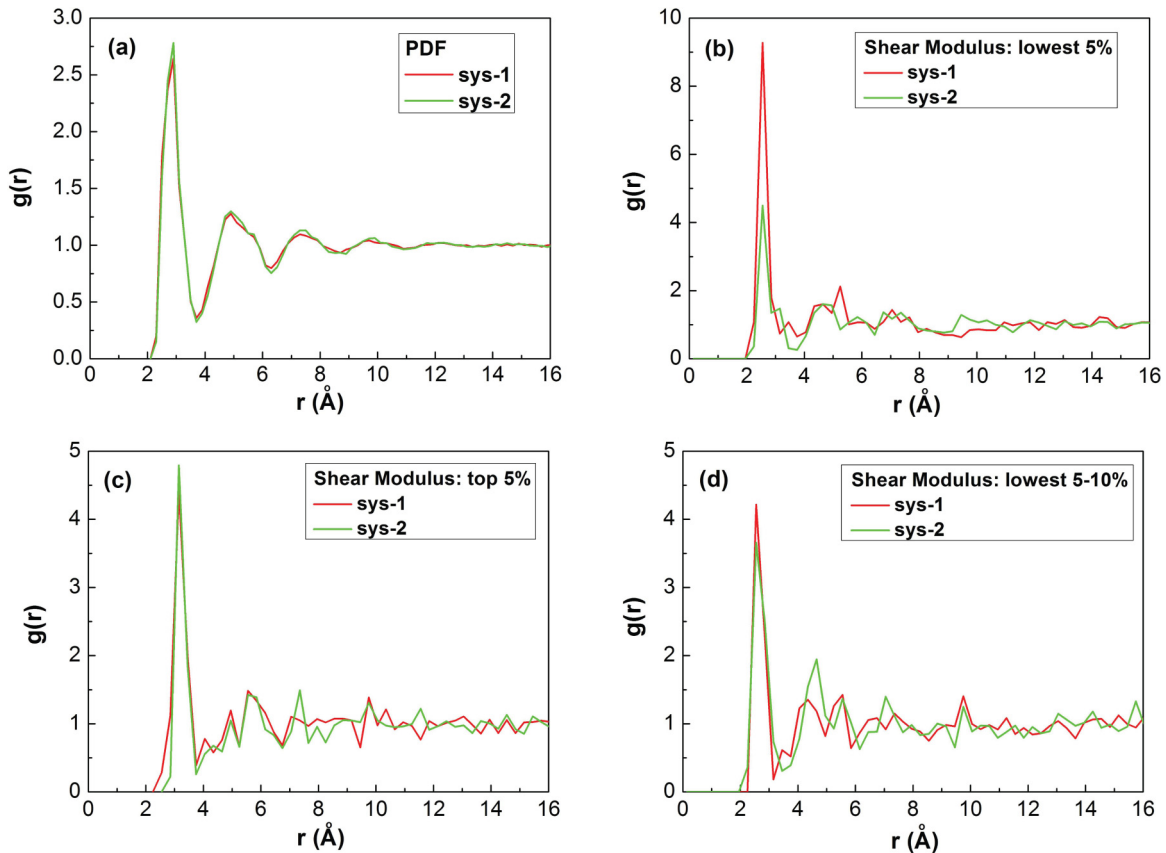
FIG. 2. (Color online) (a) The overall pair distribution function (PDF) of two systems. (b) The PDF of a subset group of atoms with lowest 5% shear modulus in two systems. (c) The PDF of the atoms with highest 5% shear modulus. (d) The PDF for the atoms with lowest 5%–10% shear modulus. Red (dark) curves are for system I, green (light) curves are for system II.
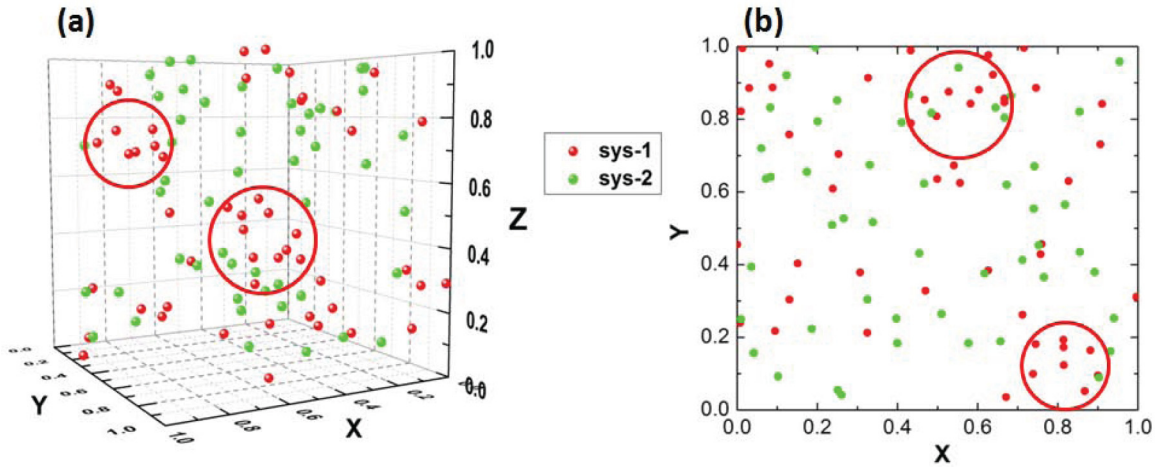
FIG. 3. (Color online) The positions of the atoms with the lowest 2.5% shear modulus, in 3D display (a), and 2D projection in X-Y plane (b). Atoms in red (dark) are for system I, and atoms in green (light) are for system II.

rates, the low-energy activations are expected to be further suppressed [22], and eventually leads to a so-called "pseudo-gap" predicted earlier [23]. Despite the significant difference in dynamic properties, the two systems have similar overall pair distribution functions (PDF), as shown in Fig. 2(a). For the more stable system II the peaks in the PDF are slightly taller and narrower than in system I, as observed experimentally in the structural relaxation [24,25]. Interestingly, however, more significant differences are found by observing the PDF through different windows. In Fig. 2(b) we show the PDF among a subset group of atoms in the systems, the PDF among the atoms with the atomic-level shear modulus in the lowest 5%, the "soft" atoms. It can be seen that the first peaks are quite different between systems I and II. The partial PDF of system I shows a strong first peak, which is twice as high as that of system II. This implies that in system I soft atoms tend to have other soft atoms as neighbors, and tend to cluster together. On the other hand, the PDFs of the atoms with the shear modulus in the highest 5% are similar in both systems, as shown in Fig. 2(c). We also examined the PDFs for the atoms with the shear modulus in the second lowest 5%–10% range in Fig. 2(d). The two systems again show similar behavior in this window. We also made similar analysis of the PDFs through other windows, in terms of the atomic-level stress and bulk

modulus, and did not observe significant differences (see the Appendix A 2 for details).

By comparing Figs. 2(b)–2(d), it is evident that the structural differences between the two systems are mainly in the distribution of the soft atoms with the shear modulus in the lowest 5%. For system I, the very tall first peak indicates clustering, while the smaller and more normal magnitude in system II represents a more homogenous distribution. To see this clustering more directly, we show the positions of the soft atoms in Figs. 3(a) and 3(b). To help guide the eyes we only display the atoms with the shear modulus in the lowest 2.5%. Figure 3(a) is the 3D illustration, whereas Fig. 3(b) is the 2D projection in the X-Y plane. It can be seen that the distribution is strongly heterogeneous for system I. Evidently the atoms are clustered, which produces the high peak in the PDF in Fig. 2(b). On the other hand, the soft atom distribution in system II is more homogenous, and therefore results in a smaller peak in the PDF.

In Fig. 4(a) we show the histograms of the atomic-level shear modulus for both systems. The average values and standard deviations are 39.62 ± 8.65 GPa (system I), and 40.24 ± 8.32 GPa (system II), respectively. The more stable system gives a higher average shear modulus (by 1.6%), and a smaller deviation (by 4.0%) as expected. However, the differences are quite small and the two systems overall show
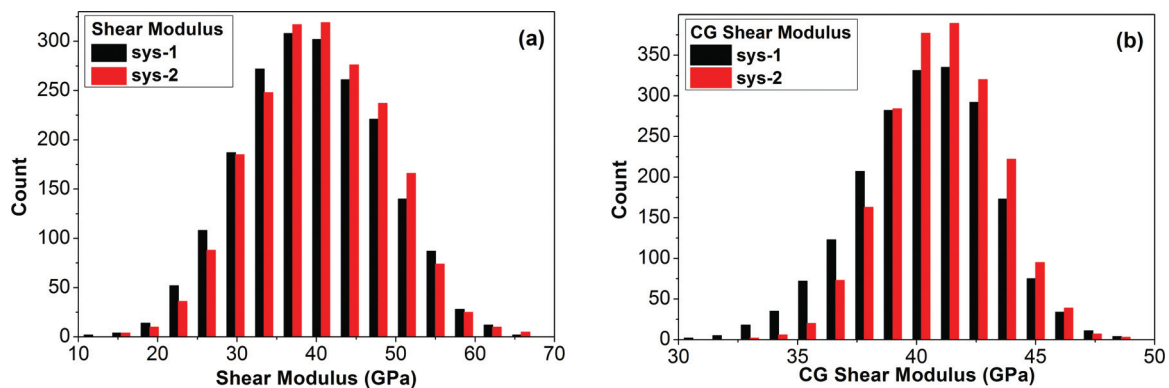
FIG. 4. (Color online) (a) The distributions of the single atomic shear modulus in both systems. (b) The distribution of the first nearest neighbor coarse-grained (CG) shear modulus, in both systems. Black (dark) bars are for system I, and red (light) bars represent system II.

similar distributions of single atomic properties. As mentioned earlier in this paper, during the activation process in ART we selected an atom as the central atom, and then introduced a random perturbation to it and its first nearest neighbors. We can thus define a local coarse-grained (CG) shear modulus as an average value of the shear moduli for this atom and its first nearest neighbors. In Fig. 4(b) we show the histograms of the local CG shear modulus. Compared to the single-atom distributions in Fig. 4(a), the distributions are narrower as a consequence of coarse graining. At the same time, in contrast to the single-atomic shear modulus distributions in Fig. 4(a), the local CG shear modulus distributions show significant difference between the two systems. The average values and standard deviations for the local CG shear modulus are 40.37 ± 2.79 GPa (system I) and 41.03 ± 2.34 GPa (system II), respectively. While the difference in the average value remains small (the difference is only around 1.6%), the local CG shear modulus distribution is much narrower, by 16.1%, in system II than in system I. The narrowness of distribution indicates system II has a reduced degree of elastic heterogeneity. In particular, as seen in Fig. 4(b), the CG shear modulus distribution at the low end is significantly suppressed in system II, whereas the distributions of the CG shear modulus at the high end do not show much difference. This interesting result is exactly the reflection of different distributions of soft atoms between the two systems, as shown in Figs. 2(b), 2(c), 3(a), and 3(b). In system I, because there are clustering of soft atoms, the CG shear modulus distribution is extended to low values and shows a long tail. In system II soft atoms are distributed more homogenously, which leads to the suppression of the low CG shear modulus distributions and stabilization of the system. Such results are in accordance with the idea that the mechanical properties of metallic glass are determined by the tail of the structural spectrum [26]. On the other hand, the hard atom distributions are similar in both systems, as seen in Fig. 2(c), so that there are no significant differences in the CG shear modulus distributions at the high end.

By comparing Figs. 4(a) and 4(b) it can be seen that the stability of amorphous material is more strongly affected by the manner with which atoms are organized, rather than the single atomic properties. In other words, even if the single atomic properties are similar, the overall properties of the systems can be quite distinct from each other when the atoms are arranged differently. Particularly in the current study, the spatial distribution of low atomic shear modulus is more heterogeneous in system I than in a more stable system II. Elastic heterogeneity in glasses is well documented [7–11]. For example, the recent study on a 2D Lennard-Jones glass by Tsamados *et al.* [7] shows strong heterogeneity of local shear modulus distribution in the flowing states driven by shear deformation, although their definition of local modulus is not exactly the same as ours. However, the difference in the spatial correlations among the soft atoms and the elastic heterogeneity evolutions between the stable and less stable system has not been observed until the present study. We demonstrate that the spatial distribution of the atoms with the lowest 5% atomic shear modulus directly reflects the difference in the stability, even though the statistical distribution of the single atomic level shear modulus is rather insensitive. In particular, these atoms become more spatially homogeneous for a more stable system.

IV. DISCUSSION AND CONCLUSION

It is also worth discussing the connection between the current study and other concepts which have been developed for a glass system. Cheng *et al.* showed that the stability of metallic glasses is strongly related to the fractions of different local topologies [27–29], i.e., less symmetric topologies are more frequently found in the inherent structures of liquids than those of glasses. Maeda *et al.* [30] demonstrated the less symmetric topologies mainly come from the regions with low shear modulus, therefore the current study is consistent with the results by Cheng *et al.* In addition, because the definition of atomic elastic moduli [14] is quite general, it can be developed into generalized quantitative models more easily, comparing with the discrete nature of topological classification [26]. On the other hand, Widmer-Cooper *et al.* showed in a 2D glass-forming liquid system, there exist causal correlations between the localized "soft modes" and system's dynamics [31]. It would therefore be of interest to study the relation between the localized soft modes and atomic modulus distribution in the future.

To conclude, we have compared the structures between two metallic glass systems with different stabilities. Although the overall structures are quite similar, the differences in the spatial distributions of atoms with shear modulus in the lowest 5% make the entire systems significantly different in terms of stability and dynamics. These results suggest an alternative way to unravel the mysterious structure-property relation in amorphous materials, by selecting appropriate windows.

ACKNOWLEDGMENTS

APPENDIX

1. Derivations of atomic level stress and modulus

a. Pair potential case

For pair interaction case, the potential energy of the system can be written as

$$E_{\text{pair}}(\{\vec{r}^{3N}\}) = \frac{1}{2} \sum_{i,j} \phi_{ij}(r_{ij}). \quad (A1)$$

Assume the system undergoes a homogeneous strain ε^{ab}, then the length change for each atom pair would be

$$\Delta r_{ij} = \frac{1}{r_{ij}} \sum_{a,b} r_{ij}^a r_{ij}^b \varepsilon^{ab}$$

$$+ \frac{1}{2r_{ij}} \sum_{a,b,c,d} \left(r_{ij}^b r_{ij}^d \delta_{ac} - \frac{1}{r_{ij}^2} r_{ij}^a r_{ij}^b r_{ij}^c r_{ij}^d \right) \varepsilon^{ab} \varepsilon^{cd}$$

$$+ O(\varepsilon^3). \quad (A2)$$

Therefore the potential energy of the system can be expanded as

$$
\Delta E_{\text{pair}} = \frac{1}{2} \sum_{i,j} \sum_{a,b} \frac{f_{ij}}{r_{ij}} r_{ij}^a r_{ij}^b \varepsilon^{ab}
$$
$$
+ \frac{1}{4} \sum_{i,j} \sum_{a,b,c,d} \left[\left(\frac{1}{r_{ij}^2} \frac{\partial f_{ij}}{\partial r_{ij}} - \frac{f_{ij}}{r_{ij}^3} \right) r_{ij}^a r_{ij}^b r_{ij}^c r_{ij}^d \right.
$$
$$
\left. + \frac{f_{ij}}{r_{ij}} r_{ij}^b r_{ij}^d \delta_{ac} \right] \varepsilon^{ab} \varepsilon^{cd} + O(\varepsilon^3), \quad (A3)
$$

where $f_{ij} = \frac{\partial \phi_{ij}(r_{ij})}{\partial r_{ij}}$.

Now assume the energy expansion can be written as

$$
\Delta E_{\text{pair}} = \sum_i \sum_{a,b} v_i \sigma_i^{ab} \varepsilon^{ab} + \frac{1}{2} \sum_i \sum_{a,b,c,d} v_i C_i^{abcd} \varepsilon^{ab} \varepsilon^{cd}
$$
$$
+ O(\varepsilon^3), \quad (A4)
$$

where σ_i^{ab} is atomic level stress, C_i^{abcd} is atomic level elastic constant, and v_i is atomic volume. By comparing Eqs. (A3) and (A4), the expression of atomic level stress and modulus for the pair potential case can thus be given as [13,14]

$$
\sigma_i^{ab} = \frac{1}{2v_i} \sum_j \frac{f_{ij}}{r_{ij}} r_{ij}^a r_{ij}^b, \quad (A5)
$$

$$
C_i^{abcd} = \frac{1}{2v_i} \sum_j \left[\left(\frac{1}{r_{ij}^2} \frac{\partial f_{ij}}{\partial r_{ij}} - \frac{f_{ij}}{r_{ij}^3} \right) r_{ij}^a r_{ij}^b r_{ij}^c r_{ij}^d + \frac{f_{ij}}{r_{ij}} r_{ij}^b r_{ij}^d \delta_{ac} \right]. \quad (A6)
$$

b. EAM potential case

In metal system, many-body interactions are widely considered, e.g., in embedded atom method (EAM) potential. In the present work we employ an EAM potential developed by Sheng *et al.* [12], which has the following formalism:

$$
E(\{\vec{r}^{3N}\}) = \sum_i F(\bar{\rho}_i) + \frac{1}{2} \sum_{i,j} \phi_{ij}(r_{ij}),
$$
$$
\bar{\rho}_i = \sum_j \rho_j(r_{ij}), \quad (A7)
$$

where $F(\bar{\rho}_i) = F[\sum_j \rho_j(r_{ij})]$ represents the many-body interactions.

Similarly as above, Eq. (A7) can be expanded with respect to a homogeneous strain ε^{ab}. Since the pair interaction contributions have been given above in Appendix A 1 *a* already, the following derivations are only focused on the many-body interactions term $E_{M.B.} = \sum_i F(\bar{\rho}_i)$.

The density change $\Delta \bar{\rho}_i$ can be expanded as a function of Δr_{ij},

$$
\Delta \bar{\rho}_i = \sum_j \frac{\partial \rho_j}{\partial r_{ij}} \Delta r_{ij} + \frac{1}{2} \sum_j \frac{\partial^2 \rho_j}{\partial r_{ij}^2} \Delta r_{ij}^2 + O(\Delta r_{ij}^3),
$$
$$
\Delta \bar{\rho}_i^2 = \sum_{j,k} \frac{\partial \rho_j}{\partial r_{ij}} \frac{\partial \rho_k}{\partial r_{ik}} \Delta r_{ij} \Delta r_{ik} + O(\Delta r_{ij}^3). \quad (A8)
$$

There is then

$$
\Delta F(\bar{\rho}_i) = \frac{\partial F}{\partial \bar{\rho}_i} \Delta \bar{\rho}_i + \frac{1}{2} \frac{\partial^2 F}{\partial \bar{\rho}_i^2} \Delta \bar{\rho}_i^2 + O(\Delta \bar{\rho}_i^3)
$$
$$
= \sum_j \frac{\partial F}{\partial \bar{\rho}_i} \frac{\partial \rho_j}{\partial r_{ij}} \Delta r_{ij} + \frac{1}{2} \sum_j \frac{\partial F}{\partial \bar{\rho}_i} \frac{\partial^2 \rho_j}{\partial r_{ij}^2} \Delta r_{ij}^2
$$
$$
+ \frac{1}{2} \sum_{j,k} \frac{\partial^2 F}{\partial \bar{\rho}_i^2} \frac{\partial \rho_j}{\partial r_{ij}} \frac{\partial \rho_k}{\partial r_{ik}} \Delta r_{ij} \Delta r_{ik} + O(\Delta r_{ij}^3). \quad (A9)
$$

Put Eq. (A2) into Eq. (A9), the many-body energy change $\Delta E_{\text{MB}} = \sum_i \Delta F(\bar{\rho}_i)$ can thus be written as strain ε^{ab}.

The first order expansion is given by

$$
\Delta E_{\text{MB}}^{(1)} = \sum_{i,j} \sum_{a,b} \frac{\partial F}{\partial \bar{\rho}_i} \frac{\partial \rho_j}{\partial r_{ij}} \frac{r_{ij}^a r_{ij}^b}{r_{ij}} \varepsilon^{ab}. \quad (A10a)
$$

Following such an expression, Nishimura *et al.* [32] and Cheng *et al.* [33] defined the atomic level stress as

$$
\sigma_i^{ab} = \frac{1}{v_i} \sum_j \frac{\partial F}{\partial \bar{\rho}_i} \frac{\partial \rho_j}{\partial r_{ij}} \frac{r_{ij}^a r_{ij}^b}{r_{ij}}. \quad (A11a)
$$

On the other hand, Eq. (A10a) can be written in a more symmetric expression as

$$
\Delta E_{\text{MB}}^{(1)} = \sum_{i,j} \sum_{a,b} \frac{\partial F}{\partial \bar{\rho}_i} \frac{\partial \rho_j}{\partial r_{ij}} \frac{r_{ij}^a r_{ij}^b}{r_{ij}} \varepsilon^{ab}
$$
$$
= \frac{1}{2} \sum_{i,j} \sum_{a,b} \left(\frac{\partial F}{\partial \bar{\rho}_i} \frac{\partial \rho_j}{\partial r_{ij}} + \frac{\partial F}{\partial \bar{\rho}_j} \frac{\partial \rho_i}{\partial r_{ij}} \right) \frac{r_{ij}^a r_{ij}^b}{r_{ij}} \varepsilon^{ab}. \quad (A10b)
$$

Transferring Eq. (A10a) to (A10b) is not only mathematically symmetric, but more importantly, Eq. (A10b) has a much clearer physical meaning. With EAM potential, the force on atom i due to atom j (only consider the many-body term) is

$$
f_{ij} = \frac{\partial F}{\partial \bar{\rho}_i} \frac{\partial \rho_j}{\partial r_{ij}} + \frac{\partial F}{\partial \bar{\rho}_j} \frac{\partial \rho_i}{\partial r_{ij}}.
$$

Therefore the term inside the parentheses in Eq. (A10b) is essentially f_{ij}. Following Eq. (A10b), the atomic level stress can thus be defined as

$$
\sigma_i^{ab} = \frac{1}{2v_i} \sum_j \left(\frac{\partial F}{\partial \bar{\rho}_i} \frac{\partial \rho_j}{\partial r_{ij}} + \frac{\partial F}{\partial \bar{\rho}_j} \frac{\partial \rho_i}{\partial r_{ij}} \right) \frac{r_{ij}^a r_{ij}^b}{r_{ij}}
$$
$$
= \frac{1}{2v_i} \sum_j f_{ij} \frac{r_{ij}^a r_{ij}^b}{r_{ij}}. \quad (A11b)
$$

It can be easily seen that the definition of Eq. (A11b) has a very clear physical meaning, and is consistent with the expression in pair potential case, as Eq. (A5). It is worth stressing that this definition is different from a previous expression.

Now proceed with second order expansion, there is

$$
\Delta E_{\mathrm{MB}}^{(2)} = \frac{1}{2} \sum_{i,j} \sum_{a,b,c,d} \frac{\partial F}{\partial \bar{\rho}_i} \frac{\partial \rho_j}{\partial r_{ij}} \frac{r_{ij}^b r_{ij}^d}{r_{ij}} \delta^{ac} \varepsilon^{ab} \varepsilon^{cd}
$$

$$
+ \frac{1}{2} \sum_{i,j} \sum_{a,b,c,d} \left(\frac{\partial F}{\partial \bar{\rho}_i} \frac{\partial^2 \rho_j}{\partial r_{ij}^2} - \frac{\partial F}{\partial \bar{\rho}_i} \frac{\partial \rho_j}{\partial r_{ij}} \frac{1}{r_{ij}} \right)
$$

$$
\times \frac{r_{ij}^a r_{ij}^b r_{ij}^c r_{ij}^d}{r_{ij}^2} \varepsilon^{ab} \varepsilon^{cd}
$$

$$
+ \frac{1}{2} \sum_{i,j,k} \sum_{a,b,c,d} \frac{\partial^2 F}{\partial \bar{\rho}_i^2} \frac{\partial \rho_j}{\partial r_{ij}} \frac{\partial \rho_k}{\partial r_{ik}} \frac{r_{ij}^a r_{ij}^b r_{ik}^c r_{ik}^d}{r_{ij} r_{ik}} \varepsilon^{ab} \varepsilon^{cd}.
$$

(A12a)

Following such an expression, the atomic level elastic constant can be defined as [32,33]

$$
C_i^{abcd} = \frac{1}{v_i} \sum_j \left[\left(\frac{\partial F}{\partial \bar{\rho}_i} \frac{\partial^2 \rho_j}{\partial r_{ij}^2} \frac{1}{r_{ij}^2} - \frac{\partial F}{\partial \bar{\rho}_i} \frac{\partial \rho_j}{\partial r_{ij}} \frac{1}{r_{ij}^3} \right) r_{ij}^a r_{ij}^b r_{ij}^c r_{ij}^d \right.
$$

$$
\left. + \frac{\partial F}{\partial \bar{\rho}_i} \frac{\partial \rho_j}{\partial r_{ij}} \frac{r_{ij}^b r_{ij}^d}{r_{ij}} \delta^{ac} \right]
$$

$$
+ \frac{1}{v_i} \sum_{j,k} \frac{\partial^2 F}{\partial \bar{\rho}_i^2} \frac{\partial \rho_j}{\partial r_{ij}} \frac{\partial \rho_k}{\partial r_{ik}} \frac{r_{ij}^a r_{ij}^b r_{ik}^c r_{ik}^d}{r_{ij} r_{ik}}. \quad (A13a)
$$

Similarly as mentioned above, there is still no clear physical meaning in the definition of Eq. (A13a). On the other hand, Eq. (A12a) can also be rewritten in a more symmetric and

physical way as

$$
\Delta E_{\mathrm{MB}}^{(2)} = \frac{1}{4} \sum_{i,j} \sum_{a,b,c,d} \left(\frac{\partial F}{\partial \bar{\rho}_i} \frac{\partial \rho_j}{\partial r_{ij}} + \frac{\partial F}{\partial \bar{\rho}_j} \frac{\partial \rho_i}{\partial r_{ij}} \right) \frac{r_{ij}^b r_{ij}^d}{r_{ij}} \delta^{ac} \varepsilon^{ab} \varepsilon^{cd}
$$

$$
+ \frac{1}{4} \sum_{i,j} \sum_{a,b,c,d} \left\{ \left[\left(\frac{\partial F}{\partial \bar{\rho}_i} \frac{\partial^2 \rho_j}{\partial r_{ij}^2} + \frac{\partial^2 F}{\partial \bar{\rho}_i^2} \frac{\partial \rho_j}{\partial r_{ij}} \frac{\partial \rho_j}{\partial r_{ij}} \right) \right. \right.
$$

$$
+ \frac{\partial F}{\partial \bar{\rho}_j} \frac{\partial^2 \rho_i}{\partial r_{ij}^2} + \frac{\partial^2 F}{\partial \bar{\rho}_j^2} \frac{\partial \rho_i}{\partial r_{ij}} \frac{\partial \rho_i}{\partial r_{ij}} \right)
$$

$$
\left. - \left(\frac{\partial F}{\partial \bar{\rho}_i} \frac{\partial \rho_j}{\partial r_{ij}} + \frac{\partial F}{\partial \bar{\rho}_j} \frac{\partial \rho_i}{\partial r_{ij}} \right) \frac{1}{r_{ij}} \right] \frac{r_{ij}^a r_{ij}^b r_{ij}^c r_{ij}^d}{r_{ij}^2} \varepsilon^{ab} \varepsilon^{cd} \right\}
$$

$$
+ \frac{1}{2} \sum_{i,j,k}^{j \neq k} \sum_{a,b,c,d} \frac{\partial^2 F}{\partial \bar{\rho}_i^2} \frac{\partial \rho_j}{\partial r_{ij}} \frac{\partial \rho_k}{\partial r_{ik}} \frac{r_{ij}^a r_{ij}^b r_{ik}^c r_{ik}^d}{r_{ij} r_{ik}} \varepsilon^{ab} \varepsilon^{cd}.
$$

(A12b)

Because with EAM potential, as mentioned above, there are

$$
f_{ij} = \frac{\partial F}{\partial \bar{\rho}_i} \frac{\partial \rho_j}{\partial r_{ij}} + \frac{\partial F}{\partial \bar{\rho}_j} \frac{\partial \rho_i}{\partial r_{ij}}
$$

and

$$
\frac{\partial f_{ij}}{\partial r_{ij}} = \frac{\partial F}{\partial \bar{\rho}_i} \frac{\partial^2 \rho_j}{\partial r_{ij}^2} + \frac{\partial^2 F}{\partial \bar{\rho}_i^2} \frac{\partial \rho_j}{\partial r_{ij}} \frac{\partial \rho_j}{\partial r_{ij}} + \frac{\partial F}{\partial \bar{\rho}_j} \frac{\partial^2 \rho_i}{\partial r_{ij}^2}
$$

$$
+ \frac{\partial^2 F}{\partial \bar{\rho}_j^2} \frac{\partial \rho_i}{\partial r_{ij}} \frac{\partial \rho_i}{\partial r_{ij}},
$$

Eq. (A12b) therefore has a much clearer physical meaning than Eq. (A12a). Following Eq. (A12b), the atomic level elastic
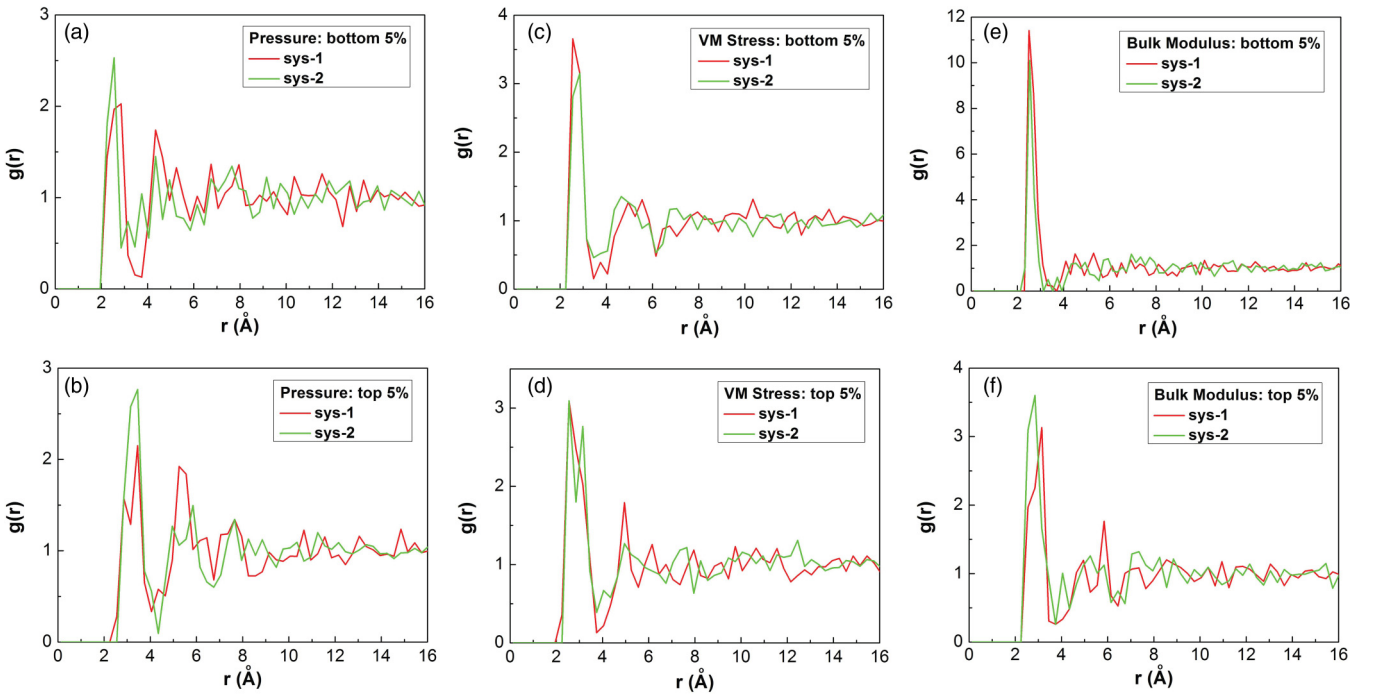
FIG. 5. (Color online) (a) and (b) The PDFs of two subsets of atoms with lowest 5% and highest 5% atomic pressure, respectively. (c) and (d) The PDFs of two subsets of atoms with lowest 5% and highest 5% atomic von Mises stress, respectively. (e) and (f) The PDFs of two subsets of atoms with lowest 5% and highest 5% bulk modulus, respectively.

constant can be then defined as

$$C_i^{abcd} = \frac{1}{2v_i} \sum_j \left[\left(\frac{1}{r_{ij}^2} \frac{\partial f_{ij}}{\partial r_{ij}} - \frac{f_{ij}}{r_{ij}^3} \right) r_{ij}^a r_{ij}^b r_{ij}^c r_{ij}^d + \frac{f_{ij}}{r_{ij}} r_{ij}^b r_{ij}^d \delta_{ac} \right]$$

$$+ \frac{1}{v_i} \sum_{j,k}^{j \neq k} \frac{\partial^2 F}{\partial \bar{\rho}_i^2} \frac{\partial \rho_j}{\partial r_{ij}} \frac{\partial \rho_k}{\partial r_{ik}} \frac{r_{ij}^a r_{ij}^b r_{ik}^c r_{ik}^d}{r_{ij} r_{ik}}. \quad (A13b)$$

It can be seen that, in such definition, the atomic level elastic constant can be divided into a two-body term and a three-body term. The two-body term has a very clear physical meaning and is in the identical formalism as the pair potential case in Eq. (A6). But such physical meaning is missing in the previous definition Eq. (A13a).

In Eqs. (A11b) and (A13b) the atomic volume v_i can be calculated either by Voronoi cells [26] or pair distances [34]. Or alternatively, following Levashov *et al.*'s recent work [35], one can redefine the atomic level stress and elastic constant elements by

$$\hat{\sigma}_i^{ab} = \frac{\sigma_i^{ab} v_i}{V/N}, \quad (A14a)$$

$$\hat{C}_i^{abcd} = \frac{C_i^{abcd} v_i}{V/N}, \quad (A14b)$$

where V is the total volume of the simulation cell, and N is the total number of atoms.

In the present work, all relevant calculations are based on Eqs. (A14a) and (A14b), and the contributions from both pair potential part [Eqs. (A5) and (A6)] and many-body part [Eqs. (A11b) and (A13b)] have been considered.

2. Pair distribution functions (PDF) through different windows

In the main text we showed the PDF of different subsets of atoms with different atomic shear modulus. We also did similar analysis through the windows, in terms of atomic stress (including the pressure and von Mises stress) and bulk modulus, as shown below. In Fig. 5 we show the PDFs of subsets of atoms with the lowest 5% and highest 5% atomic pressure [Figs. 5(a) and 5(b)], von Mises stress [Figs. 5(c) and 5(d)], and bulk modulus [Figs. 5(e) and 5(f)], respectively. It can be seen that there are no remarkable differences between the PDFs, which implies insignificant correlations between the distributions of these properties and the stabilities of the systems.

[1] P. W. Anderson, Science **267**, 1615 (1995).
[2] P. G. Debenedetti and F. H. Stillinger, Nature (London) **410**, 259 (2001).
[3] S. Sastry, P. G. Debenedetti, and F. H. Stillinger, Nature (London) **393**, 554 (1998).
[4] D. Rodney and C. Schuh, Phys. Rev. Lett. **102**, 235503 (2009).
[5] H. Kallel, N. Mousseau, and F. Schiettekatte, Phys. Rev. Lett. **105**, 045503 (2010).
[6] A. Kushima, X. Lin, J. Li, J. Eapen, J. C. Mauro, X. Qian, P. Diep, and S. Yip, J. Chem. Phys. **130**, 224504 (2009).
[7] M. Tsamados, A. Tanguy, C. Goldenberg, and J.-L. Barrat, Phys. Rev. E **80**, 026112 (2009).
[8] H. Mizuno, S. Mossa, and J.-L. Barrat, Phys. Rev. E **87**, 042306 (2013).
[9] M. Hideyuki, M. Stefano, and B. Jean-Louis, Europhys. Lett. **104**, 56001 (2013).
[10] H. Wagner, D. Bedorf, S. Küchemann, M. Schwabe, B. Zhang, W. Arnold, and K. Samwer, Nat. Mater. **10**, 439 (2011).
[11] F. Leonforte, R. Boissière, A. Tanguy, J. P. Wittmer, and J. L. Barrat, Phys. Rev. B **72**, 224206 (2005).
[12] Y. Q. Cheng, E. Ma, and H. W. Sheng, Phys. Rev. Lett. **102**, 245501 (2009).
[13] T. Egami, K. Maeda, and V. Vitek, Philos. Mag. A **41**, 883 (1980).
[14] T. Egami and D. Srolovitz, J. Phys. F: Metal Phys. **12**, 2141 (1982).
[15] G. T. Barkema and N. Mousseau, Phys. Rev. Lett. **77**, 4358 (1996).
[16] E. Cancès, F. Legoll, M.-C. Marinica, K. Minoukadeh, and F. Willaime, J. Chem. Phys. **130**, 114711 (2009).
[17] T. Iwashita, D. M. Nicholson, and T. Egami, Phys. Rev. Lett. **110**, 205504 (2013).
[18] D. Rodney, A. Tanguy, and D. Vandembroucq, Model. Simul. Mater. Sci. Eng. **19**, 083001 (2011).
[19] T. Zhu, J. Li, A. Samanta, A. Leach, and K. Gall, Phys. Rev. Lett. **100**, 025502 (2008).
[20] Y. Fan, Y. N. Osetsky, S. Yip, and B. Yildiz, Phys. Rev. Lett. **109**, 135503 (2012).
[21] Y. Fan, Y. N. Osetskiy, S. Yip, and B. Yildiz, Proc. Natl. Acad. Sci. U.S.A. **110**, 17756 (2013).
[22] P. Koziatek, J.-L. Barrat, P. Derlet, and D. Rodney, Phys. Rev. B **87**, 224105 (2013).
[23] T. Egami, J. Alloys Compd. **434-435**, 110 (2007).
[24] T. Egami, J. Mater. Sci. **13**, 2587 (1978).
[25] D. Srolovitz, T. Egami, and V. Vitek, Phys. Rev. B **24**, 6936 (1981).
[26] Y. Q. Cheng, J. Ding, and E. Ma, Mater. Res. Lett. **1**, 3 (2013).
[27] Y. Q. Cheng, A. J. Cao, and E. Ma, Acta Mater. **57**, 3253 (2009).
[28] Y. Q. Cheng, H. W. Sheng, and E. Ma, Phys. Rev. B **78**, 014207 (2008).
[29] Y. Q. Cheng and E. Ma, Prog. Mater. Sci. **56**, 379 (2011).
[30] K. Maeda and S. Takeuchi, Philos. Mag. A **44**, 643 (1981).
[31] A. Widmer-Cooper, H. Perry, P. Harrowell, and D. R. Reichman, Nat. Phys. **4**, 711 (2008).
[32] M. Nishimura, K. Yashiro, and M. Arai, J. Soc. Mater. Sci. Jpn. **59**, 631 (2010).
[33] Y. Q. Cheng and E. Ma, Phys. Rev. B **80**, 064104 (2009).
[34] V. A. Levashov, T. Egami, R. S. Aga, and J. R. Morris, Phys. Rev. B **78**, 064205 (2008).
[35] V. A. Levashov, J. R. Morris, and T. Egami, Phys. Rev. Lett. **106**, 115703 (2011).